Triple-Resonance $^{19}F,^{1}H,^{13}C$ CPMAS NMR Study of the Influence of PMMA Tacticity on the Miscibility in PMMA/PVF_2 Blends

A. P. A. M. Eijkelenboom, W. E. J. R. Maas, and W. S. Veeman*

Department of Molecular Spectroscopy, Faculty of Science, University of Nijmegen, Toernooiveld, 6525 ED Nijmegen, The Netherlands

G. H. Werumeus Buning and J. M. J. Vankan

Philips Research Laboratories, P.O. Box 80.000, 5600 JA Eindhoven, The Netherlands

Received November 20, 1991

ABSTRACT: Molecular miscibility in blends of poly(methyl methacrylate) (PMMA) with poly(vinylidene fluoride) (PVF_2) with isotactic, syndiotactic, and atactic PMMA was investigated by triple-resonance $^{1}H,^{19}F,^{13}C$ solid-state CPMAS NMR. From the fluorine to carbon cross polarization experiments the average distance between fluorines and OCH_3 carbons in intimately mixed PVF_2 and PMMA was estimated. Experimental evidence for a specific interaction between PVF_2 and PMMA segments is presented. The proton to fluorine cross depolarization experiments yield information on size and composition of the mixed PMMA/PVF_2 phase. The fraction of nonmixed PMMA was determined for these blends, and it was found that this fraction was smaller for isotactic than for atactic and syndiotactic PMMA. Large differences in the amounts of isolated PMMA are observed between melt-mixed and coprecipitated blends.

1. Introduction

The miscibility of poly(methyl methacrylate) (PMMA) with poly(vinylidene fluoride) (PVF_2) has been established by various methods.[1-9] The presence of interchain interactions is believed to be a prerequisite for miscibility in polymer blends.[10] Léonard et al.[7] showed, using FTIR, that the miscibility of PMMA and PVF_2 is promoted by hydrogen bonding between the protons of PVF_2 and the carbonyl oxygen of PMMA. The presence of strong interactions that lead to the observed miscibility is indicated by the negativity of the interaction parameter χ_{12}, which has been determined by various methods such as melting point depression studies,[1-3] SANS,[4] SAXS,[5] and inverse gas chromatography.[6]

In this study the influence of PMMA tacticity on molecular miscibility in PMMA/PVF_2 blends is investigated. It may be expected that polymer microstructure will affect both the nature of specific interactions and the composition of the mixed phase in polymer blends. Stejskal et al.[11] showed differences in proton $T_{1\rho}$ relaxation behavior between blends of poly(phenylene oxide) and atactic polystyrene (PPO/a-PS) as compared to blends of PPO and isotactic PS (PPO/i-PS). Schurer et al.[12] observed two glass transition temperatures for blends of isotactic PMMA and poly(vinyl chloride) (PVC) over the entire composition range, indicating nonmiscibility for this blend. In contrast, blends of syndiotactic PMMA and PVC exhibited a single T_g up to 60 wt % s-PMMA.

The influence of PMMA tacticity on the miscibility in PMMA/PVF_2 blends has been investigated by studying the melting point depressions of the PVF_2 crystalline phase in these blends.[2,13] PMMA samples with different tacticity exhibit strong differences in flexibility.[13,14] This behavior is reflected in different NMR longitudinal relaxation times, both in solution[14] and in the solid state,[15,16] and in strongly varying glass transition temperatures of the stereoisomers. For the materials used here, we found with DSC that T_g = 58 °C for isotactic (i) and 138 °C for syndiotactic (s) PMMA. Upon blending with PVF_2 (T_g = −30 °C), the glass transition temperature for a given composition is thus lower for i-PMMA/PVF_2 than for s-PMMA/PVF_2. As a consequence, the crystallization behavior of PVF_2 is different in these blends. Furthermore, the interchain interactions between PMMA and PVF_2, which depress the melting point of PVF_2 crystallites, result in a negative energy of mixing, which stabilizes the blend. Melting point depression data indicate stronger interactions of PVF_2 with i-PMMA than with a-PMMA or s-PMMA.[2,13]

Two previously introduced solid-state CPMAS NMR techniques are used here to investigate the influence of PMMA tacticity on molecular miscibility in amorphous PMMA/PVF_2 blends. The $^{19}F-^{13}C$ cross polarization technique[8] is used to examine the nature of specific interactions as a function of PMMA tacticity, while the $^{1}H-^{19}F$ cross depolarization technique[9] is used to determine the composition and nature of the miscible domains. These techniques will be discussed below.

2. Experimental Section

A. Materials. The a-PMMA used was PMMA 6N from Röhm GmbH (Darmstadt, FRG). This polymer contains 10% methyl acrylate groups. Its average molecular weight $\bar{M}_w$, determined with GPC relative to polystyrene standards, was 100 000. The i-PMMA and s-PMMA used were kindly provided by Prof. G. E. Challa and Mr. J. Vorenkamp of the State University of Groningen (The Netherlands). Their average molecular weights $\bar{M}_w$ are 275 000 and 66 000, respectively. The PVF_2 used was Kynar homopolymer grade 401 with an average molecular weight $\bar{M}_w$ of 530 000 (Pennwalt). The tacticities of the PMMA samples were determined by ^{1}H NMR in $CDCl_3$. For a-PMMA, the presence of methyl acrylate resonances was ignored. The triad percentages are given in Table I.

B. Blend Preparation. Blends were prepared via coprecipitation and subsequent compression molding, as described by Roerdink and Challa.[2] The PMMA/PVF_2 weight composition was 60/40 for all blends. For this composition ratio of the blend, 7.5 g of the mixture was dissolved in 250 g of DMF (Merck). The solution was added dropwise to 3 L of water. The precipitated mixture was filtered off and dried at high vacuum for a minimum of 6 days at 50 °C and for several hours at 160 °C to remove the last traces of solvent. The dried mixture was then molded in a press at 200 °C prior to quenching from the melt in liquid nitrogen. The T_g's found (DSC, heating rate 20 °C/min) for the different blends and their homopolymers are listed in Table II.

C. NMR. Experiments were performed on a Bruker CXP 300 spectrometer, operating at 300.1, 282.2, and 75.4 MHz for ^{1}H, ^{19}F, and ^{13}C NMR, respectively. A standard Bruker double-bearing MAS probehead was used. The triple tuning of the probe-

0024-9297/92/2225-4511$03.00/0

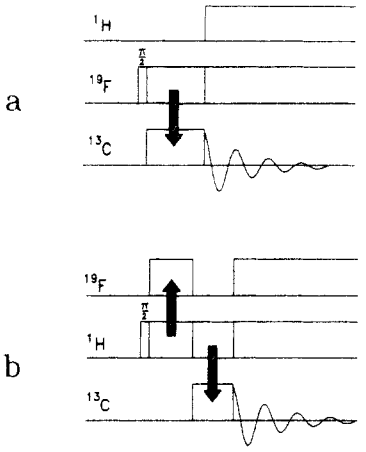

Figure 1. Pulse sequences for (a) ^{19}F–^{13}C cross polarization and (b) ^1H–^{19}F cross depolarization experiments.

Table I
Triad Percentages of the PMMA Homopolymers

	triad		
	isotactic (mm)	heterotactic (mr)	syndiotactic (rr)
i-PMMA	96	4	0
a-PMMA	5	34	61
s-PMMA	1	9	90

Table II
Glass Transition Temperatures T_g of the Various PMMA/PVF_2 60/40 Blends and Their Homopolymers

homopolymer	T_g (K)	blend	T_g (K)
i-PMMA	331	i-PMMA/PVF_2	311
a-PMMA	379	a-PMMA/PVF_2	343
s-PMMA	411	s-PMMA/PVF_2	359
PVF_2	243		

head was achieved by using a previously described setup.[8] Magic angle spinning rates were 5 kHz in the fluorine to carbon cross polarization experiments and 3.5 kHz in the proton to fluorine cross depolarization experiments. Rf field strengths were typically 50 kHz on protons, fluorines, and carbon. Carbon free induction decays were acquired under simultaneous proton and fluorine high-power decoupling. In experiments involving cross polarization, spin temperature alternation was used. All experiments were performed at room temperature.

In Figure 1a, the pulse scheme for the ^{19}F–^{13}C cross polarization experiment is depicted. A $\pi/2$ pulse at the ^{19}F frequency is applied prior to a Hartmann–Hahn matched spin-lock on ^{19}F and ^{13}C during a variable time t, in which fluorine magnetization can be transferred to carbons. Subsequently, the carbon magnetization is detected.

Figure 1b shows the pulse scheme for the ^1H–^{19}F cross depolarization experiment. A $\pi/2$ pulse at the ^1H frequency is applied prior to a Hartmann–Hahn matched spin lock on ^1H and ^{19}F during a variable time t, in which protons can lose their magnetization to the fluorines. Subsequently, the remaining proton magnetization is transferred to carbons via ^1H–^{13}C cross polarization during 1 ms and the carbon magnetization is detected. To prevent fluorine magnetization from building up during the first step of the experiment, the phase of the fluorine rf field is shifted every 50 μs.

3. Results

^{19}F–^{13}C Cross Polarization. In the ^{19}F–^{13}C cross polarization (CP) experiments magnetization is transferred from fluorines to carbons via their mutual dipolar coupling. Magnetization transfer is therefore limited to nuclei that are near each other. In a ^{19}F–^{13}C CP experiment on PMMA/PVF_2 blends a PMMA carbon signal will only be observed from PMMA segments that are within a few angstroms from PVF_2 fluorines.[8]

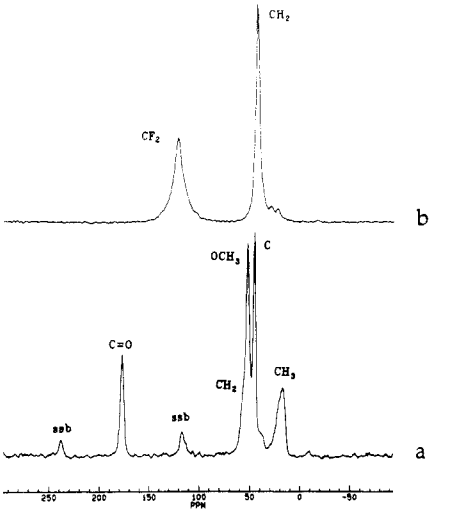

Figure 2. ^{13}C MAS spectra obtained by ^1H–^{13}C cross polarization of (a) atactic PMMA, acquired with proton decoupling, and (b) PVF_2, acquired with simultaneous proton and fluorine decoupling.

Figure 2 shows the carbon spectra of PMMA and PVF_2 and the assignment of the resonances. As can be seen from these spectra, the PMMA methoxy and carbonyl resonances are suitable to monitor the PMMA magnetization in the blends, since they do not overlap with PVF_2 resonances. The ^{19}F–^{13}C cross polarization spectra of i-PMMA/PVF_2, a-PMMA/PVF_2, and s-PMMA/PVF_2 are shown in Figure 3. In all spectra PMMA resonances are observed, indicating molecular miscibility in all blends. To obtain information on the distance between a PVF_2 fluorine and a PMMA carbon, a series of experiments was performed with variable ^{19}F–^{13}C cross polarization times. Figure 4 shows the peak intensities of the OCH_3 carbon resonance of i-PMMA/PVF_2, a-PMMA/PVF_2, and s-PMMA/PVF_2 as a function of the contact time. The data are fitted with the following equation:[17]

$$S(t) = \frac{S_0}{a_+ - a_-}\left[\exp\left(\frac{-a_- t}{T_{IS}}\right) - \exp\left(\frac{-a_+ t}{T_{IS}}\right)\right] \qquad (1)$$

in which

$$a_\pm = a_0[1 \pm (1 - b/a_0^2)^{1/2}]$$

$$a_0 = \frac{1}{2}\left(1 + \epsilon + \frac{T_{IS}}{T_{1\rho}{}^I} + \frac{T_{IS}}{T_{1\rho}{}^S}\right)$$

$$b = \frac{T_{IS}}{T_{1\rho}{}^I}\left(1 + \frac{T_{IS}}{T_{1\rho}{}^S}\right) + \epsilon\frac{T_{IS}}{T_{1\rho}{}^S}$$

$$\epsilon = \frac{N_S S(S+1)}{N_I I(I+1)}$$

and where S_0 is the maximum carbon magnetization available in a cross polarization process without dissipative processes. $T_{1\rho}{}^I$ and $T_{1\rho}{}^S$ are the rotating frame spin–lattice relaxation time constants for the I and S spins, respectively, and T_{IS} is the cross polarization time constant.

The rotating frame relaxation times ^{19}F $T_{1\rho}$ and ^{13}C $T_{1\rho}$ are measured in separate experiments. The ^{19}F $T_{1\rho}$'s are determined via a ^{19}F–^{13}C cross polarization experiment in which the fluorine magnetization is transferred to the carbons at the end of a variable-time ^{19}F spin lock. The ^{13}C $T_{1\rho}$'s are measured in a ^1H–^{13}C cross polarization experiment in which the carbon spin-lock field is continued for a variable time after turning off the proton rf field. With the values obtained, the data of Figure 4 were fitted

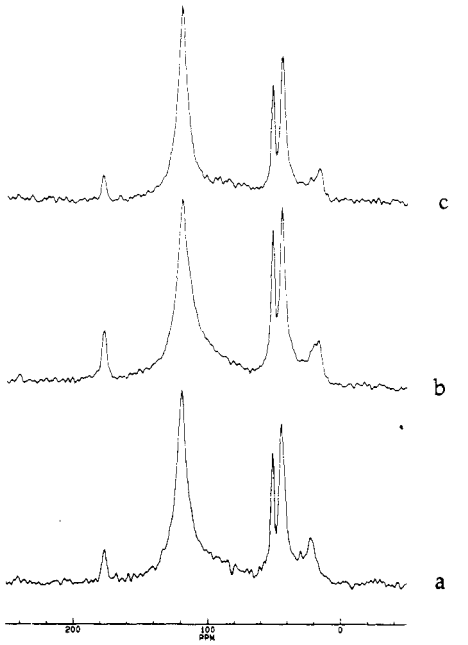

Figure 3. $^{19}F-^{13}C$ CPMAS spectra of (a) isotactic, (b) atactic, and (c) syndiotactic PMMA/PVF_2 60/40 blends.

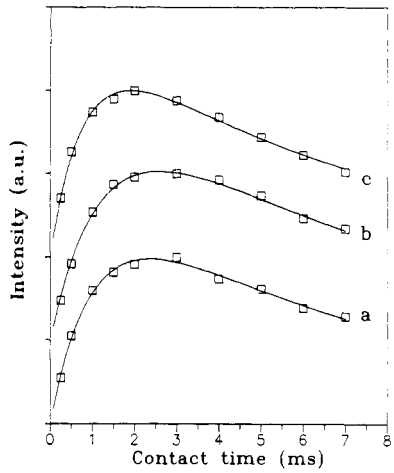

Figure 4. $^{19}F-^{13}C$ CP OCH_3 carbon intensities of (a) isotactic, (b) atactic, and (c) syndiotactic PMMA/PVF_2 60/40 blends fitted with a single T_{IS}^{-1} value.

Table III
Cross Polarization Parameters for the OCH_3 Carbon for Different PMMA/PVF_2 60/40 Blends

	T_{IS} (ms)	$T_{1\rho}^F$ (ms)	$T_{1\rho}^C$ (ms)	r_{av} (Å)	Gaussian fit σ (Å)	Gaussian fit r_{av}^* (Å)
i-PMMA/PVF_2	8 ± 2	1.1 ± 0.2	50 ± 5	2.9 ± 0.1	0.2	3.0 ± 0.1
a-PMMA/PVF_2	10 ± 2	1.1 ± 0.2	80 ± 5	3.0 ± 0.1	0.2	3.1 ± 0.1
s-PMMA/PVF_2	7 ± 2	1.1 ± 0.2	85 ± 5	2.8 ± 0.1	0.2	2.8 ± 0.1

with eq 1, resulting in a cross relaxation time T_{IS}. In this way, T_{IS} was determined for the C=O and OCH_3 resonances for all blends. The parameters are summarized in Table III for the OCH_3 resonance and apply to the C=O carbon as well.

Extracting Spatial Information from T_{IS}. The T_{IS}^{-1} values can be used to obtain spatial information under the assumption that the cross polarization dynamics can be described by a single transfer rate. This assumption seems reasonable since the cross polarization curves (Figure 4) are satisfactorily fitted by the calculated curves, but a different approach will be described later in this section. The value of T_{IS}^{-1} can be related to the average $^{19}F-^{13}C$ distance, as was described previously.[8] If both spins are irradiated at resonance and if the Hartmann–Hahn condition is fulfilled, the cross relaxation rate can be approximated in the high effective field approximation according to Demco et al.[18] as

$$T_{IS}^{-1} = {}^1/_4\pi^{1/2}\tau_c M_{2,SI} \quad (2)$$

in which τ_c is the fluorine spin–spin fluctuation correlation time and $M_{2,SI}$ is the second moment of the carbon spins due to coupling with fluorine spins. This second moment describes the local field of the carbon spins due to the presence of nearby fluorines. If there is no preferential orientation of the internuclear vectors with respect to the magnetic field, as in polycrystalline or amorphous solids, the second moment can be expressed as

$$M_{2,SI} = {}^4/_{15}\gamma_I^2\gamma_S^2\hbar^2 I(I+1)\sum_{I,S} r_{IS}^{-6} \quad (3)$$

If T_{IS} is known for a given S spin, it is possible to calculate the average $\langle r_{IS}^{-6}\rangle = \sum_{I,S} r_{IS}^{-6}$, from which an average distance $\langle r_{IS}\rangle$ may be approximated:

$$T_{IS}^{-1} \sim \langle r_{IS}^{-6}\rangle \quad (4)$$

This value of $\langle r_{IS}\rangle$ is a weighted average and will be mainly determined by the shortest I–S distances, due to the dependence of the second moment on the distance to the inverse sixth power.

To calculate the average $^{19}F-^{13}C$ distances in the PMMA/PVF_2 blends a value for the correlation time τ_c is needed. For these blends this value has been estimated from the cross polarization curve of the CF_2 resonance of PVF_2 in the blends. We assume the directly bonded fluorines are primarily responsible for the cross polarization of the CF_2 carbons. From the known $^{19}F-^{13}C$ distance (1.34 Å) τ_c was determined as 1.0 ± 0.1 ms. The average distances r_{av} from PVF_2 fluorines to PMMA OCH_3 carbons found in this way are listed in Table III.

Although the experimental cross polarization data as a function of the contact time are well described by assuming a single cross relaxation time, intuitively this seems a poor approximation. In these amorphous systems one can in general expect that each individual carbon spin experiences a different local field, due to the nearby presence (or absence) of fluorine spins. For each microscopic environment a second moment of the S spins is determined by the proximity of I spins, and for each of these segments an average $\langle r_{IS}^{-6}\rangle$ can be defined. For the amorphous blends used in this study this means a distribution of second moments. Since it is still reasonable to assume that all segments have a random orientation with respect to the magnetic field direction, a powder average can again be taken, which leads to a distribution in $\langle r_{IS}^{-6}\rangle$ and in $M_{2,SI}$. The observed S-spin magnetization as a function of cross polarization time t is thus a summation over microscopic magnetization curves:

$$(T_{IS}^{-1})_{local} \sim \langle r_{IS}^{-6}\rangle_{local} \quad (5)$$

$$S(t) = \sum_n W_n(r)\, S_n(t,(T_{IS}^{-1})_{local}) \quad (6)$$

The weighted summation of individual cross polarization curves S_n runs over the possible microscopic segments, multiplied by a probability factor $W_n(r)$, and can be restricted to segments with a nonnegligible value of $\langle r_{IS}^{-6}\rangle_{local}$. Equation 6 was used to fit the experimental cross polarization data. T_{IS}^{-1} values are calculated for distances ranging from 2.8 up to 10 Å. The minimum distance was chosen just below the sum of the van der Waals radii of a fluorine atom in PVF_2 and a carbon in PMMA. According to the equation for nonbonded in-

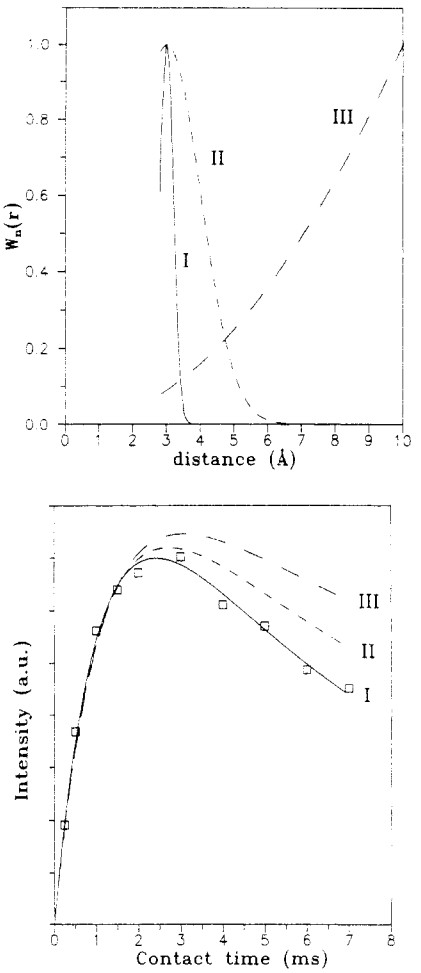

Figure 5. (a) Narrow Gaussian (I), broad Gaussian (II), and spherical (III) distribution functions. (b) OCH_3 intensities of i-PMMA/PVF_2 fitted with the distribution function of a.

teractions given by Loufakis et al.,[19] the ^{19}F–^{13}C interaction is repulsive only below this minimum distance. Several shapes of the distribution function $W_n(r)$ were used to fit the experimental data. Some examples are shown in Figure 5a. Figure 5b depicts the best fit to the OCH_3 carbon intensities of i-PMMA/PVF_2, obtained with the distribution functions of Figure 5a. Two of the distribution functions are Gaussians, one with a broad distribution (σ = 1.0 Å) around an average distance and one with a narrow distribution (σ = 0.2 Å). The third function expresses that in a completely amorphous structure all ^{19}F–^{13}C distances are possible and that the probability of finding a certain distance r increases with r^2. Good data fits are only obtained by assuming a narrow Gaussian distribution function, around a distance r_{av}* that is close to the average distance r_{av} found by assuming a single value of T_{IS}^{-1}. This result, obtained from experimental data from methoxy as well as from carbonyl resonances, applies to all blends studied (see Table III). The PMMA carbons observed in the ^{19}F–^{13}C cross polarization experiment apparently experience a similar local field, induced by nearby fluorine spins. *The fact that the observed data cannot be approximated by either a broad or a random distribution leads us to conclude that a specific interaction must exist between segments of PMMA and PVF_2.*

^1H–^{19}F Cross Depolarization. In the ^{19}F–^{13}C CP experiments described above, the buildup of PMMA carbon magnetization is restrained due to the short ^{19}F $T_{1\rho}$ compared to the cross polarization time constant T_{IS}. This prevents us from accurately determining the amount of PMMA that is intimately mixed with PVF_2. Instead of using the fluorines as a source of magnetization, as was the case in the ^{19}F–^{13}C cross polarization technique, we now use the fluorine reservoir as a sink, through which proton magnetization can disappear.[9]

If, after creation of spin-locked proton magnetization in the whole sample, a fluorine rf field is turned on, its strength adjusted to the proton–fluorine Hartmann–Hahn condition, then all the protons that have a dipolar interaction with fluorines will lose their magnetization to the lattice via the fluorines. In a second step the remaining proton magnetization is transferred to carbons via ^1H–^{13}C cross polarization, and the carbon magnetization is detected (see Figure 1b). The observed PMMA carbon magnetization is then from parts of PMMA chains whose protons do *not* have a dipolar interaction with fluorine. In other words, only those parts of PMMA molecules that are remote from PVF_2 molecules are observed.

In performing this ^1H–^{19}F cross depolarization experiment, the short fluorine $T_{1\rho}$ is an advantage in that it makes the fluorine reservoir act as a good sink for proton magnetization. This sink function can even be improved, either by applying a phase-modulated rf field[20] or by frequently switching the phase of the rf fields by 180°, as was done in this experiment. To determine the amount of PMMA that is close to PVF_2, a blank experiment was performed, which is similar to the experiment depicted in Figure 1b, except that no fluorine rf field was used. If we denote the proton signal from the depolarization experiment S_A and the signal from the blank experiment S_B, the observed signals can be equated as

$$S_A(t) = S_0 f_{mix} \exp\left(\frac{-t}{T_{1\rho}}\right) D(t) + S_0(1 - f_{mix}) \exp\left(\frac{-t}{T_{1\rho}}\right) \quad (7)$$

$$S_B(t) = (S_0 f_{mix} + S_0(1 - f_{mix})) \exp\left(\frac{-t}{T_{1\rho}}\right) \quad (8)$$

in which S_0 is the total proton magnetization, f_{mix} is the fraction of protons close to fluorines, and $D(t)$ is a decaying function which describes the loss of magnetization due to depolarization to the fluorine sink.

By dividing both signals, we have corrected for loss of magnetization to the lattice, characterized by the proton $T_{1\rho}$:

$$S_A(t)/S_B(t) = f_{mix} D(t) + (1 - f_{mix}) \quad (9)$$

By transferring at time t the proton magnetization to carbon, the proton signal $S_A(t)/S_B(t)$ can be mapped out via the carbon resonances of PMMA or PVF_2.

In Figure 6 the carbon spectra of the blends are shown, obtained by cross polarization from protons (with depolarization time t = 0). A proton–fluorine cross depolarization experiment was performed as described above. The OCH_3 carbon intensities as a function of the depolarization time are shown in Figure 7. The magnetization decay curves level off to nearly constant values. These levels are attributed to PMMA that is remote from PVF_2 and therefore this PMMA is classified as not mixed. The curves show that the amount of isolated PMMA in the case of i-PMMA/PVF_2 (4%) is less than for a-PMMA/PVF_2 (9%) and s-PMMA/PVF_2 (12%).

Apart from the fraction of isolated PMMA in the blends, information on the amount of isolated PVF_2 and on the composition of the domains in which PMMA and PVF_2 are intimately mixed can be extracted from the cross depolarization experiments. A model has recently been introduced[9] that takes into account the proton spin diffusion as well as the losses of proton magnetization to the fluorine sink. In this model the blend is assumed to consist of four phases.

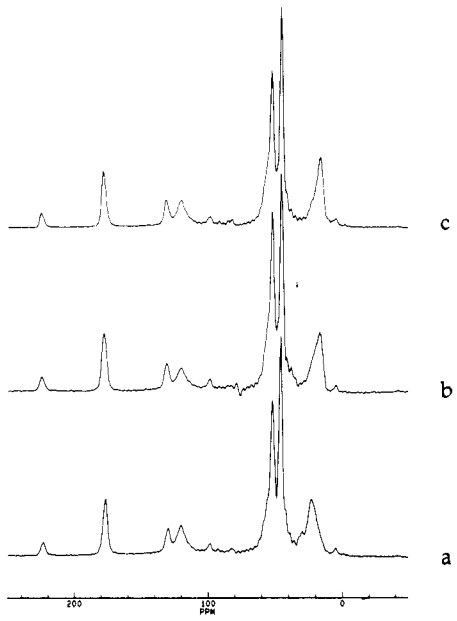

Figure 6. ^1H–^{13}C CPMAS spectra of (a) isotactic, (b) atactic, and (c) syndiotactic PMMA/PVF_2 60/40 blends.

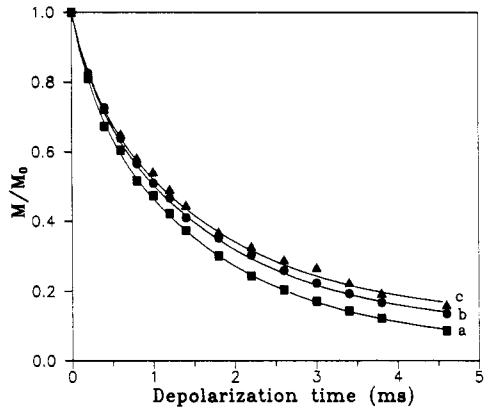

Figure 7. ^1H–^{19}F cross depolarization OCH_3 carbon intensities of (a) isotactic, (b) atactic, and (c) syndiotactic PMMA/PVF_2 60/40 blends. The solid lines are calculated spin diffusion curves.

Phase I consists of isolated PVF_2 and is characterized by the fact that no PMMA proton magnetization can diffuse into this region on the time scale of the experiment. PVF_2 protons in this phase lose their proton magnetization to the fluorines with a rate constant T_{HF}^{-1} which is assumed to be equal to that in pure PVF_2, and this fraction can therefore simply be determined.

Phase II contains PMMA and PVF_2 that are intimately mixed. Protons in this phase transfer their magnetization directly to fluorines with a rate constant $(T_{HF}^{eff})^{-1}$, which differs from T_{HF}^{-1} because of the presence of PMMA.

Phase III is assumed to contain PMMA close to the mixed phase (II), so that it will lose proton magnetization not directly to the fluorine sink but via proton spin diffusion to the mixed phase.

Phase IV is an isolated PMMA phase whose proton magnetization is not affected by depolarization nor by spin diffusion. As a result this phase will show up as an offset in the cross depolarization data of Figure 7, as has already been mentioned above.

Since the proton magnetization is detected via ^{13}C, the magnetization behavior of PMMA and PVF_2 belonging to the different phases can be monitored separately: the PVF_2 present in phases I and II is represented by the CF_2 resonance, whereas the decays of the carbonyl, methoxy, and methyl resonances of PMMA represent PMMA in phases II and III. The isolated PMMA and PVF_2 fractions can be determined directly from the experimental data.

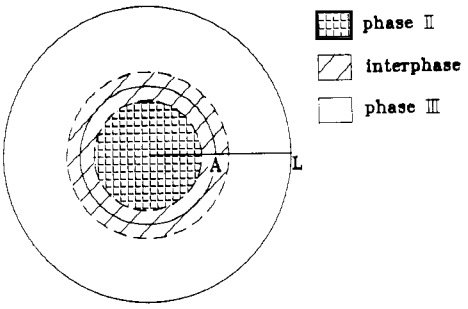

Figure 8. Distribution of phases II and III as used in the spin diffusion model.

The behavior of the magnetization as a function of the depolarization time can be described by a spherical isotropic spin diffusion equation for the mixed PMMA/PVF_2 phase II and the neighboring PMMA phase III:

$$\frac{\partial C(r,t)}{\partial t} = D\frac{\partial^2 C(r,t)}{\partial r^2} + f(r)\, C(r,t) \qquad (10)$$

in which $C(r,t)$ is the magnetization concentration at time t and site r, D is the diffusion coefficient, which is assumed constant in the blend, and $f(r)$ is a spatial-dependent function which describes the depolarization via cross polarization as a function of the distance to the fluorine sink. $f(r)$ is zero for protons located in phase III. To model the loss of PMMA and PVF_2 proton magnetization to the fluorine sink, the values of the diffusion coefficient (D) and the rate constants for magnetization losses in the mixed phase ($(T_{HF}^{eff})^{-1}$) and in the isolated PVF_2 phase (T_{HF}^{-1}) are needed. T_{HF}^{eff} was found to be 300 μs as previously described[9] and T_{HF}, obtained from pure PVF_2, equaled 120 μs. The spin diffusion coefficient D was determined via the proton T_2's of these blends[9] and was found to be 21 Å^2/ms. The differences in mobility between blends with different stereoregular forms of PMMA, as mentioned in the Introduction, are not reflected in differences in proton T_2's, probably since all experiments are performed below the glass transition temperatures of the blends.

The spin diffusion equation (10) can be evaluated based on a previously introduced spherical diffusion model.[9] In this model, depicted in Figure 8, intimately mixed PMMA and PVF_2 (phase II) are contained in a sphere with radius A. Surrounding this phase is an outer sphere with radius L, which consists of PMMA (phase III). In the inner sphere proton magnetization will be directly transferred to fluorines via cross polarization. Subsequently, there will be a flow of magnetization from PMMA protons, located in the surrounding sphere, to protons in the inner sphere via spin diffusion, for which radial spin diffusion is assumed. Numerical evaluation of the spin diffusion equation with the above-mentioned parameters and for different values of A and L yields curves that can be fitted to the experimental depolarization data. The details of these calculations are described elsewhere.[9]

As shown in Figure 7, the calculated solid lines represent the experimental data well with A = 7 or 8 Å and L = 14 or 15 Å for i-PMMA/PVF_2 and A = 6 or 7 Å and L = 13 or 14 Å for a-PMMA/PVF_2 and s-PMMA/PVF_2. Other PMMA carbon resonances yield the same values for A and L.

The magnetization decays observed for the PVF_2 CF_2 carbon resonance of the blends arise from PVF_2 that is intimately mixed with PMMA and from isolated PVF_2. The calculated curves should therefore be composed of a curve affected by spin diffusion and an exponential decay

Table IV
Fractions of PMMA and PVF_2 That Are Not Mixed and Monomer Ratios (MR) in the Blend and in the Mixed Phase

	PMMA/PVF_2 60/40		
	i-PMMA/ PVF_2	a-PMMA/ PVF_2	s-PMMA/ PVF_2
% PMMA not mixed	4	9	12
% PVF_2 not mixed	5	15	15
total MR	0.96	0.96	0.96
MR in mixed region	0.97	1.03	0.99

curve with a rate constant T_{HF}^{-1}, which is obtained from pure PVF_2.[9] For i-PMMA/PVF_2 the CF_2 carbon data are fitted with the same values of A and L used to fit the PMMA carbon data and with 5% PVF_2 contained in the isolated phase (the data are not shown here). Slightly larger values for L are needed to fit the CF_2 data for a- and s-PMMA/PVF_2 (A = 6 Å, L = 15 Å), and in both blends 15% of the PVF_2 was not mixed. The results are summarized in Table IV. If one considers material contained in a sphere with radius L as intimately mixed, the PMMA/PVF_2 monomer ratio (MR) in this mixed phase can be calculated since the fractions of isolated PMMA and PVF_2 are known. The calculated values are also listed in Table IV. This monomer ratio is close to one for all blends studied.

All experimental results can be fitted by the four-phase model. The results all suggest $A = 7 \pm 1$ Å and $L = 14 \pm 1$ Å. The question whether these dimensions are related to real physical dimensions of domains or whether they are imposed by the cross relaxation and spin diffusion mechanisms will be addressed later.

4. Discussion

The ^{19}F–^{13}C cross polarization experiments provide information on nearest-neighbor distances between PVF_2 fluorines and PMMA carbons. A good description of the experimental data is obtained only by assuming either a single carbon–fluorine distance (see Figure 4) or a narrow distribution of distances (Figure 5). These findings strongly indicate a specific interaction between PMMA segments and PVF_2 segments. Moreover, the estimated distances (about 3 Å) are close to the sum of the van der Waals radii. (The reported van der Waals radii of PMMA are 1.7 Å for a carbonyl carbon, 1.9 Å for an ester CH_3 group,[21] and 1.3 Å for a PVF_2 fluorine.[19])

The ^{19}F–^{13}C cross polarization experiments do not reveal differences between blends with different stereoregular PMMA configurations. This means that the nature of the interactions between PVF_2 and PMMA segments is not influenced by the tacticity of PMMA.

It was shown by Léonard et al.[7] that hydrogen bonding between PVF_2 protons and carbonyl oxygens of PMMA is the main cause of molecular interactions between these polymers. The number of contacts between such unlike chains will depend on the relative conformations of the respective segments.

For PMMA both energy calculations and experimental results indicate a strong preference for an all-trans conformation, irrespective of tacticity.[22–26] PVF_2 adopts short sequences of all-trans (tt) or trans–gauche (tg) conformation.[19,13] The PVF_2 tt conformation allows more efficient interactions with PMMA than the tg counterpart. Léonard et al.[13] noted that the spacing between CH_2 groups in the PVF_2 tt conformation nearly matches the spacing between successive carbonyl groups of PMMA. The occurrence of a hydrogen bond would then position adjacent CH_2 groups close to carbonyl groups, which enables multiple contacts. These multiple interactions stabilize the PVF_2 all-trans conformation as evidenced by an increase in trans/gauche ratio as a function of the PMMA content in PMMA/PVF_2 blends.[13] Evidence for multiple contacts was also reported by Saito et al.,[27] whose depolarized light scattering experiments revealed short-range ordering in PMMA/PVF_2 blends due to local chain alignments.

Apart from PMMA in the all-trans conformation also a small fraction of tg conformational diads is present. These fractions are visible in the ^1H–^{13}C CPMAS NMR spectra of the blends (see Figure 6). The effect is most pronounced in the case of isotactic PMMA. In the spectrum of the i-PMMA/PVF_2 blend the CH_3 carbon region exhibits two resonances, a strong resonance at 23 ppm and a weak resonance at approximately 30 ppm. Spěváček et al.[15] attributed the largest resonance to the tt conformation and the smaller one to tg conformational diads. The latter is shifted with respect to the tt resonance due to the so-called γ-gauche effect. The shoulder on the left side of the CH_3 resonance in s-PMMA and the asymmetric shape of the CH_3 resonance in a-PMMA are also attributed to the presence of tg conformations. Surprisingly, these resonances are also observed in the ^{19}F–^{13}C cross polarization spectra (Figure 3). This could be understood if one recognizes the tg conformational diads as defects with small persistence lengths between sequences of tt conformation. In that case multiple interactions between all-trans PMMA segments and PVF_2 will force parts of PVF_2 molecules to approach the PMMA tg diads. In addition, single contacts may be present.

The similarity of the nature of PMMA and PVF_2 interactions in the case of different stereoregular PMMA forms is confirmed by the ^1H–^{19}F cross depolarization experiments. The sizes A and L, used in the model to describe the loss of proton magnetization via spin diffusion to the fluorine sink, are the same for all blends studied. Also the PMMA/PVF_2 monomer ratio in the mixed phase is equal in all blends. This value is close to one, tempting one to conclude a one-to-one mixing of PMMA and PVF_2 chains. However, care must be taken in drawing such a conclusion, due to the somewhat hypothetical character of the domains involved in the proposed spin diffusion model. Apart from the nature of the interaction, the ^1H–^{19}F cross depolarization experiment provides information on the number of close PMMA and PVF_2 contacts. Differences are observed in the fractions of PMMA and PVF_2 that are not intimately mixed in the blends (see Table IV). The nonmixed fraction of PMMA in the blends increases in the order isotactic (4%), atactic (9%), and syndiotactic (12%). The same trend has been observed by Roerdink et al.[2] and Léonard et al.[13] by studying the crystallization behavior of PVF_2 in PMMA/PVF_2 blends. Their results suggest a stronger interaction of PVF_2 with isotactic than with syndiotactic and atactic PMMA.

Possible explanations for this difference are offered by differences in molecular weight, mobility, and extended chain structure between blends with PMMA of different tacticity. A possible effect of the molecular weight of PMMA on the number of interactions seems to be excluded by the agreement with the observations of Roerdink et al., who used a-PMMA of the lowest and s-PMMA of the highest molecular weight. The larger flexibility of i-PMMA as compared to the stiffer atactic and syndiotactic chains makes it easier to adopt a favorable conformation to allow for multiple interactions and to induce local chain alignments. Although the average persistence length of tt conformational diads in pure i-PMMA (about 6 backbone bonds[24]) is smaller than for s-PMMA (about 16–20

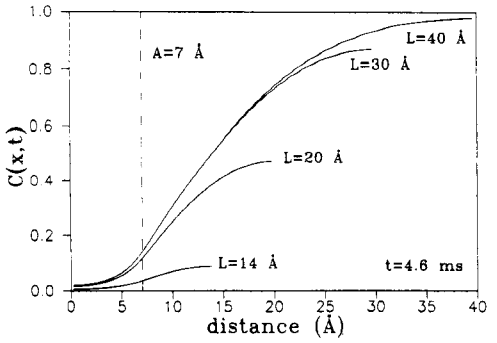

Figure 9. Magnetization concentration curves for $A = 7$ Å and different values of L at a depolarization time of 4.6 ms. The $C(x,t)$ values are calculated up to $x = L$.

backbone bonds[24,25]), this effect is probably canceled by the curvature of a- and s-PMMA chains due to unequal backbone angles.[22,25]

The results obtained from this study agree well with results obtained from other experimental techniques. The trends observed for the microscopic observation of the fraction of isolated PMMA correspond to the trends observed for the macroscopic interaction parameter χ_{12}. Roerdink and Challa[2] found χ_{12} for i-PMMA/PVF_2 (−0.13) to be smaller than for a-PMMA/PVF_2 (−0.10) and s-PMMA/PVF_2 (−0.06). The same trend is observed in the fraction of isolated PMMA in our samples. Also the finding that χ_{12} becomes less negative at larger PMMA contents, as reported by several authors,[3,4,28] is supported by our previously reported results.[9]

The domains and the dimensions A and L are introduced via a mathematical model in which the blend is assumed to consist of four phases. Two of the phases, namely the fractions of isolated PMMA and PVF_2, are determined independently of the proposed spin diffusion model. These phases are distinguished on the generally accepted criterion[11,29-32] that the proton magnetization within these phases is not affected by spin diffusion to protons in the mixed phase. It is tempting to speculate about the physical meaning of the dimensions A and L. It seems likely that the dimension A found from the fitting procedure simply expresses the fact that ^1H–^{19}F cross polarization over distances larger than A angstroms is too slow to be noticed. The dimension L may be thought of to be limited by proton spin diffusion. However, in the time available for proton spin diffusion much larger distances than L angstroms can be bridged.[29,30] This is visualized in Figure 9. In this figure the magnetization concentration $C(x,t)$ is plotted as a function of the distance from the center of the sink for $A = 7$ Å and at a time $t = 4.6$ ms. The magnetization concentration curves are calculated for several values of L. From this picture it becomes clear that for $L = 14$ Å, which is the value found by fitting the experimental data, almost all proton magnetization has diffused out of phase III into the sink. This means that $L = 14$ Å is not a limit set by spin diffusion, since we know that $C(x,t) = 1$ in order not to be affected by proton spin diffusion. For comparison also the concentration curves for $L = 20$, 30, and 40 Å are calculated. As can be seen from Figure 9 even protons at 40 Å from a fluorine sink lose magnetization due to spin diffusion, so spin diffusion is effective over distances much larger than 14 Å. We therefore cannot simply say that L has to do with the proton spin diffusion length. A likely possibility is that the dimension A of phase II describes the interacting PMMA and PVF_2 segments. In this view L would then be related to an average distance between interacting PMMA and PVF_2 pairs.

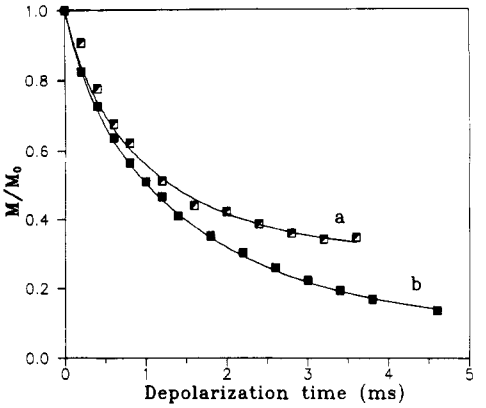

Figure 10. OCH_3 cross depolarization data for a PMMA/PVF_2 60/40 blend obtained via (a) melt mixing and (b) coprecipitation.

It is interesting to note that others have reported heterogeneities in PMMA/PVF_2 blends on comparable scales. Wendorff[5] concluded from WAXS measurements the existence of concentration fluctuations for this blend, which are correlated over distances up to 10 Å. Jamil and Jamieson[33] reported heterogeneities in PMMA/PVF_2 blends on a scale of 8.3 Å, which is the length scale of their ESR spin probe.

Finally, we briefly remark on observed differences between blends prepared by melt-kneading (Brabender W30EH) and blends cast from solution. Figure 10 shows the intensities of the PMMA OCH_3 resonances in a ^1H–^{19}F cross depolarization experiment for a melt-mixed a-PMMA/PVF_2 60/40 blend (data taken from Maas et al.[9]) and a solution-cast 60/40 blend. For the melt-mixed blend it was observed that 30% of PMMA is contained in the nonmixed phase, whereas in the solution-cast blend only 9% is not mixed. In both samples an isolated PVF_2 fraction of 15% was found. Furthermore, for PMMA/PVF_2 60/40 the monomer ratio in the mixed phase was reported to be 0.75 for the melt-mixed blend,[9] whereas a value of 1.03 is found here. No differences are observed in either the sizes (A and L) of the miscible domains or the ^{19}F–^{13}C distances, indicating that the nature of the interactions is equal for melt-mixed and solution-cast blends. Three possible explanations are offered for this behavior. The melt-kneaded blend may not have been mixed long enough to obtain complete mixing, whereas the polymers are already thoroughly mixed in solution. The differences may also be caused by dead volume in the kneading apparatus. Results of Hirata et al.[34] suggest that a lower critical solution temperature (LCST) type phase separation may have taken place in the melt-mixed blend. The observed differences in monomer ratios in the mixed regions of differently prepared blends are obviously due to differences in the number of interacting PMMA and PVF_2 segments. The larger number of contacts in the solution-cast blend than in the melt-mixed blend, as indicated by the smaller fraction of isolated PMMA, increases the amount of PMMA close to PVF_2 and therefore the monomer ratio in the mixed phase.

5. Conclusions

^{19}F–^{13}C cross polarization and ^1H–^{19}F cross depolarization NMR experiments are well suited to investigate molecular miscibility in PMMA/PVF_2 blends. From the NMR experiments the existence of a specific interaction between PMMA and PVF_2 segments is concluded. The nature of this interaction is not influenced by the tacticity of PMMA. The number of bilateral interactions in the sample seems larger in isotactic PMMA/PVF_2 samples

compared to atactic and syndiotactic PMMA/PVF_2 samples, as indicated by smaller amounts of isolated PMMA in the isotactic sample. The observed microscopic trends in this study agree well with observations by others of the macroscopic interaction parameter χ_{12}.

Acknowledgment. This work was supported by the Dutch Research Foundation (NWO/SON). We thank Mr. J. W. M. van Os, Mr. A. A. G. van Oijen, and Mrs. G. H. Nachteegaal for technical assistance at the Dutch National NMR Facility at Nijmegen. Prof. G. E. Challa and Mr. J. Vorenkamp are gratefully acknowledged for supplying the i- and s-PMMA.

References and Notes

(1) Nishi, T.; Wang, T. T. *Macromolecules* **1975**, *8*, 909.
(2) Roerdink, E.; Challa, G. *Polymer* **1978**, *19*, 173.
(3) Morra, B. S.; Stein, R. S. *J. Polym. Sci., Polym. Phys. Ed.* **1982**, *20*, 2243.
(4) Hadziioannou, G.; Stein, R. S. *Macromolecules* **1984**, *17*, 567.
(5) Wendorff, J. H. *J. Polym. Sci., Polym. Lett. Ed.* **1980**, *18*, 439.
(6) DiPaola-Baranyi, G.; Fletcher, S. J.; Degré, P. *Macromolecules* **1982**, *15*, 885.
(7) Léonard, C.; Halary, J. L.; Monnerie, L. *Polymer* **1985**, *26*, 1507.
(8) Klein Douwel, C. H.; Maas, W. E. J. R.; Veeman, W. S.; Werumeus Buning, G. H.; Vankan, J. M. J. *Macromolecules* **1990**, *23*, 406.
(9) Maas, W. E. J. R.; van der Heijden, W. A. C.; Veeman, W. S.; Vankan, J. M. J.; Werumeus Buning, G. H. *J. Chem. Phys.* **1991**, *95*, 4698.
(10) Olabisi, O.; Robeson, L. M.; Shaw, M. T. *Polymer–Polymer Miscibility*; *Springer Series in Solid-State Sciences*; Academic: New York, 1979.
(11) Stejskal, E. O.; Schaefer, J.; Sefcik, M. D.; McKay, R. A. *Macromolecules* **1981**, *14*, 275.
(12) Schurer, J. W.; de Boer, A.; Challa, G. *Polymer* **1975**, *16*, 201.
(13) Léonard, C.; Halary, J. L.; Monnerie, L. *Macromolecules* **1988**, *21*, 2988.
(14) Lyerla, J. R.; Horikawa, T. T.; Johnson, D. E. *J. Am. Chem. Soc.* **1977**, *99*, 2463.
(15) Spěváček, J.; Schneider, B.; Straka, J. *Macromolecules* **1990**, *23*, 3042.
(16) Edzes, H. T.; Veeman, W. S. *Polym. Bull.* **1981**, *5*, 255.
(17) Mehring, M. *Principles of High Resolution NMR in Solids* (Vol. 12 of *NMR—Basic Principles and Progress*), 2nd ed.; Springer-Verlag: New York, 1983.
(18) Demco, D. E.; Tegenfeldt, J.; Waugh, J. S. *Phys. Rev. B* **1975**, *11*, 4133.
(19) Loufakis, K.; Miller, K. J.; Wunderlich, B. *Macromolecules* **1986**, *19*, 1271.
(20) Stejskal, E. O.; Schaefer, J.; McKay, R. A. *J. Magn. Reson.* **1984**, *57*, 471.
(21) Bosscher, F.; ten Brinke, G.; Eshuis, A.; Challa, G. *Macromolecules* **1982**, *15*, 1364.
(22) Sundararajan, P. R.; Flory, P. J. *J. Am. Chem. Soc.* **1974**, *96*, 5025.
(23) Yoon, D. Y.; Flory, P. J. *Polymer* **1975**, *16*, 645.
(24) Yoon, D. Y.; Flory, P. J. *Macromolecules* **1976**, *9*, 299.
(25) Lovell, R.; Windle, A. H. *Polymer* **1981**, *22*, 175.
(26) Birshtein, T. M.; Merkur'yeva, A. A.; Goryunov, A. N. *Polym. Sci. USSR (Engl. Transl.)* **1983**, *25*, 143.
(27) Saito, H.; Matsuura, M.; Okada, T.; Inoue, T. *Polym. J.* **1989**, *21*, 357.
(28) Chow, T. S. *Macromolecules* **1990**, *23*, 333.
(29) Cheung, T. T. P.; Gerstein, B. C. *J. Appl. Phys.* **1981**, *52*, 5517.
(30) Havens, J. R.; VanderHart, D. L. *Macromolecules* **1985**, *18*, 1663.
(31) Caravatti, P.; Neuenschwander, P.; Ernst, R. R. *Macromolecules* **1986**, *19*, 1889.
(32) Schmidt-Rohr, K.; Clauss, J.; Blümich, B.; Spiess, H. W. *Magn. Reson. Chem.* **1990**, *28*, s3.
(33) Jamil, T.; Jamieson, A. M. *J. Polym. Sci., Part B: Polym. Phys.* **1989**, *27*, 2553.
(34) Hirata, Y.; Kotaka, T. *Polym. J.* **1981**, *13*, 273.

Registry No. PVF_2, 24937-79-9; isotactic PMMA, 25188-98-1; syndiotactic PMMA, 25188-97-0; atactic PMMA, 9011-14-7.